Desalination and Water Treatment
www.deswater.com
doi: 10.1080/19443994.2014.947779

55 (2015) 3172–3177
September

Taylor & Francis
Taylor & Francis Group

Cavitational reactor for advanced treatment of contaminated water: the effect of recovery pressure

Mauro Capocelli[a], Marina Prisciandaro[b,*], Amedeo Lancia[c], Dino Musmarra[a]

[a]*Dipartimento di Ingegneria Civile, Design, Edilizia e Ambiente, Seconda Università degli Studi di Napoli, Real Casa dell'Annunziata, via Roma 29, 81031 Aversa, Italy, Tel. +39 0817682236; email: mauro.capocelli@gmail.it (M. Capocelli), Tel. +39 0815010400; email: dino.musmarra@unina2.it (D. Musmarra)*
[b]*Dipartimento di Ingegneria Industriale, dell'Informazione e di Economia, Università dell'Aquila, viale Giovanni Gronchi 18, 67100 L'Aquila, Italy, Tel. +39 0862434241; email: marina.prisciandaro@univaq.it (M. Prisciandaro)*
[c]*Dipartimento di Ingegneria Chimica, dei Materiali e della Produzione Industriale, Università "Federico II" di Napoli, Piazzale V. Tecchio, 80, 80125 Napoli, Italy, Tel. +39 0817682243; email: lancia@unina.it (A. Lancia)*

Received 1 April 2014; Accepted 16 June 2014

ABSTRACT

This article deals with study of hydrodynamic cavitation in a Venturi reactor by considering the degradation of p-nitrophenol and the numerical simulation of a cavitating bubble in the explored experimental conditions. The parameters depicting the cavitation performances are reported for several experimental conditions. The best result of pNP mass removed at 30 min was found by setting the inlet pressure at 0.70 MPa and the recovery one at 0.38 MPa (≈40%), while the best performances in terms of pNP conversion per unit energy consumed were observed at 0.40 MPa (2.41 mg/MJ). The study represents a step forward in the work carried out by our research group to gain theoretical insight and optimize cavitation for advanced wastewater treatment.

Keywords: Hydrodynamic cavitation; Mathematical modeling; Recovery pressure; Venturi; p-Nitrophenol

1. Introduction

Cavitation is the formation, growth, and subsequent collapse of microbubbles in a liquid. These phenomena release large magnitudes of energy per unit volume over an extremely small interval of time (10^{-3} s), resulting in high local pressures (10–500 MPa) and temperatures (1,000–10,000 K). The collapses also result in the formation of highly reactive free radicals, in continuous surface and interface cleaning as well as in the enhancement of mass transfer rates due to the turbulence generated [1]. Therefore, the application of cavitation is being studied by many researchers in many fields of process intensification and, particularly, in the water treatment processes for the degradation of various organic pollutants [1–8].

In hydrodynamic cavitation (HC), the above-described phenomena are realized through constrictions such as orifice plates or Venturi. According to the

*Corresponding author.

Presented at the Conference on Desalination for the Environment: Clean Water and Energy 11–15 May 2014, Limassol, Cyprus

pertinent literature, HC (particularly if employed in hybrid techniques) is showing the lowest energy consumption among other similar Advanced Oxidation Processes (AOPs) [2,7,8]. Although there are many studies on HC, its actual implementation as a consolidated wastewater treatment technology is still an open field of research. The main strands of research are as follows: the optimization of process parameters [7,9,10], the implementation of HC in hybrid techniques to obtain higher depuration yields [4,8,10,11], and the modeling of bubble dynamics with chemical reactions in order to understand and optimize the process [12–17].

This paper is part of a wider study carried out by this research group, focused on the experimental and theoretical insight of the HC process in order to enhance the degradation of organic pollutants [5,7,13]. Particularly in this work the cavitation-mediated oxidation in a Venturi reactor is addressed by studying the decomposition of a model organic molecule (a priority pollutant), p-Nitrophenol (pNP), going into details of the effect of recovery pressure downstream the cavitation reactor. A mathematical model simulating the bubble dynamics is the instrument used to discuss the experimental evidences.

2. Experimental apparatus and procedures

Fig. 1 depicts the experimental setup: a closed-loop reactor consisting of a holding tank of 1.5 L volume with cooling system, a centrifugal pump (500–3,500 rpm, 0.4 kW) and two pipe-lines. The main line comprises the Venturi reactor and two pressure gauges provided to measure the inlet pressure (p_1) and the fully recovered downstream pressure (p_2). Two control valves enable to modulate the flow rate and the pressure drop. The inside diameter of both the main and the by-pass lines is 12 mm, further details regarding the apparatus are given in a recently published paper [9]. The valve in the by-pass line (V-1) is partially closed to adjust the inlet pressure p_1 (which is also the pump discharge pressure) on the upstream side of the orifice plate. The fully recovered pressure, p_2 on the downstream side is regulated through the valve V-2. The values of these operating variables varied in the range $p_1 = 0.20$–0.75 MPa; $p_2 = 0.10$–0.35 MPa, $Q = 0.2$–0.4 $m^3 h^{-1}$. The pNP initial concentration was 1 ppm, initial pH was 5.5; the temperature was kept below the limit of $T_w = 30$ °C during the experiments. During testing, some 1-ml samples were drawn from the test reservoir. The absorbance of pNP was monitored at 0, 5, 10, 20, 30 min. The pNP concentrations were measured using a UVV spectrophotometer following the procedures of Kotronarou et al. [18]. Reagent grade pNP, sulfuric acid, and sodium hydroxide were used for pH adjustment. The spectrophotometer was calibrated against the known concentrations of pNP in distilled water at a wavelength of 401 nm after shifting the sample pH to 11 by adding NaOH to enable measurement [18].

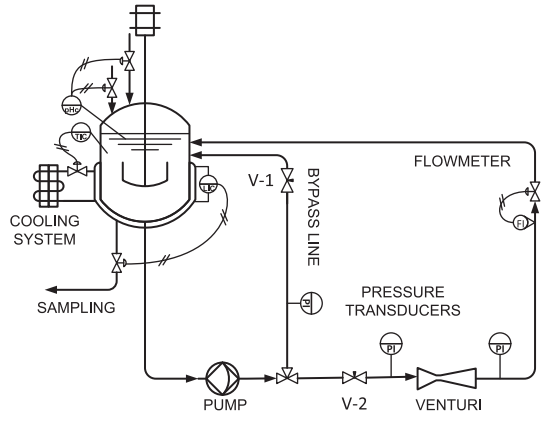

Fig. 1. Layout of the experimental apparatus.

3. Mathematical model

The mathematical model of the cavitating bubble is described by the following five ordinary differential equations, together with their initial values: Rayleigh–Plesset Eq. (1), diffusive flux of water vapor (2), energy balance of the bubble (3), continuity (4) and Bernoulli Eq. (5). The mathematical approach is in continuity with previous papers by the same research group [7,13,15] and is described in detail in a recent modeling work [2] that reports different maps of cavitation regimes obtained by varying the operating parameters. The integration domain $[0 \le x \le L]$ is the length of a cavitating device; the model also includes the estimation of turbulent fluctuation velocity for the calculation of the local velocity U, following the approach firstly proposed by Moholkar and Pandit [14]. The system of Eqs. (1–5) can be solved using the fourth-order/fifth-order Runge–Kutta–Fehlberg variable step-size method to obtain the variation of bubble radius, temperature, pressure along with the number of molecules trapped in the bubble, assuming the indicated initial values. More details on the transport properties can be found in the work of Kumar et al. [12].

$$p_l = \frac{N_{tot} kT}{4\pi(R^3 - h^3)/3} - \frac{2\sigma}{R} - \frac{4\mu U}{R}\left(\frac{dR}{dx}\right) - \rho\left[R\left(U^2\frac{d^2R}{dx^2} + U\frac{dU}{dx}\frac{dR}{dx}\right) + \frac{3U^2}{2}\left(\frac{dR}{dx}\right)^2\right] \quad (1)$$

$$R(0) = R_0; \left.\frac{dR}{dx}\right|_0 = 0$$

$$u\frac{dN_w}{dx} = 4\pi R^2 D\left(\frac{C_{wR} - C_w}{l_{diff}}\right) \quad N_w(0) = 0 \tag{2}$$

$$C_{v,mix}\frac{dT}{dx} = \frac{4\pi R^2\lambda}{u}\left(\frac{T_w - T}{l_{th}}\right) - p_i\frac{d(4\pi R^3/3)}{dx} + (h_w - U_w)\frac{dN_w}{dx} \quad T(0) = T_w \tag{3}$$

$$\left(u\frac{dA}{dx} + A\frac{du}{dx}\right)\left(1 - \frac{4\pi nR^3}{3}\right) = 4\pi n\, uAR^2\frac{dR}{dx}\; U(0) = v_o \tag{4}$$

$$U\frac{dU}{dx} = -\frac{1}{\rho(1 - 4\pi nR^3/3)}\frac{dp_l}{dx} \quad p(0) = p_v \tag{5}$$

4. Results and discussion

The experimental results of this paper can be summarized in two groups: The first one comprises the experiments aimed at analyzing the effect of the inlet pressure p_1 at the fixed recovery one p_2; the second group includes the runs carried out to evaluate the effect of the recovery pressure at a constant Venturi pressure drop. Fig. 2 reports the results belonging to the first group, showing the dimensionless concentration of pNP along with the treatment time at five different inlet pressures (p_1). The results indicated that the HC oxidation is favored by a higher p_1 until a critical pressure is reached. For the system under examination this value is *ca.* 0.40 MPa and was recognized in a previous paper in similar conditions [7], as well as in the literature for different experiments [19,20]. It can be ascribed to the establishment of a cavitating regime responsible for dumping the energy of cavitating bubbles [20]. An experimental and theoretical insight into the optimization of inlet pressure value is also given in our previous paper [9].

As already said, a second group of experiments was conducted in order to investigate the effect of recovery pressure; therefore, similar experiments were performed but at different p_2. By assuming from the previous consideration that 0.30 MPa could be an optimal pressure drop, the flow rate was adjusted in order to keep a constant pressure drop $\Delta p \approx 0.30$ MPa. The results are reported in Fig. 3 where it is possible to observe an overall increase in the removal percentage: the highest removal at 30 min is found at $p_1 = 0.70$ MPa, $p_2 = 0.38$ MPa. Table 1 summarizes the experimental parameters and quantifies some variables useful for the comparison. A key measure of the oxidation performances is the energy required to

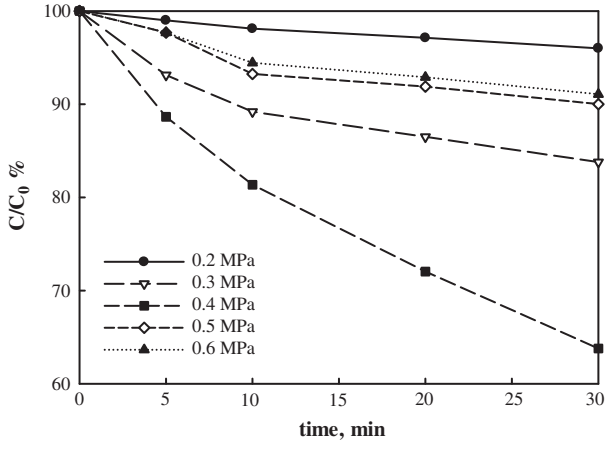

Fig. 2. pNP degradation at different inlet pressure, p_1; the recovery pressure is $p_2 = 0.10$ MPa.

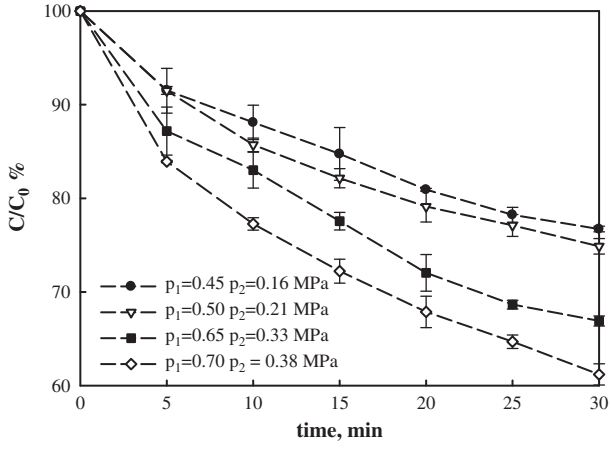

Fig. 3. pNP degradation, effect of recovery pressure p_2.

Table 1
Experimental conditions and overall performances of cavitation

p_1 MPa	p_2 MPa	C_v	C (30 min)/C_0 %	η (30 min) mg/MJ
0.20	0.10	0.57	96.00	0.67
0.30	0.10	0.44	83.78	1.61
0.40	0.10	0.36	63.78	2.41
0.50	0.10	0.29	90.00	0.48
0.60	0.10	0.25	91.06	0.33
0.45	0.16	0.52	76.72	1.30
0.50	0.21	0.63	74.88	1.21
0.65	0.33	0.77	66.90	1.08
0.70	0.38	0.82	61.20	1.13

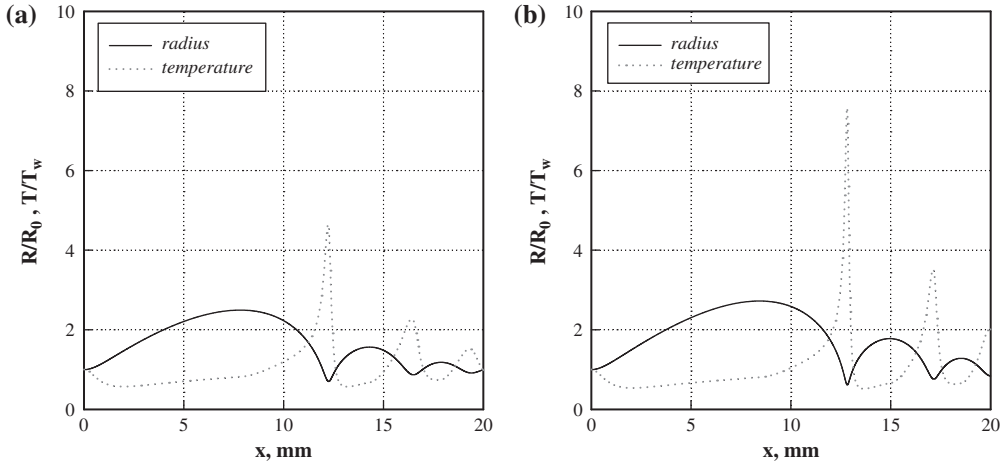

Fig. 4. Single bubble simulation, dimensionless radius and temperature. $R_0 = 5\,\mu m$, $T_w = 293\,K$. (a): $p_1 = 0.65\,MPa$, $p_2 = 0.10\,MPa$; (b): $p_1 = 0.65\,MPa$, $p_2 = 0.33\,MPa$.

remove a unit mass of a given compound. This is expressed in Eq. (6) as the cavitation efficiency η: the cumulative mass of contaminant removed per unit energy expended:

$$\eta(t) = \frac{(C_0 - C(t))V}{tP} \tag{6}$$

where C_0 is the initial concentration, $C(t)$ the concentration at time t, V the liquid volume, and P the expended power. Moreover, in Table 1 the cavitation number C_v is given for all the experiments: At similar values of C_v the increase in recovery pressure has a positive effect on the degradation rate. Nonetheless, by increasing the p_2, a little reduction of η is found with respect to the highest values observed at $p_1 = 0.40\,MPa$ and atmospheric recovery pressure. This can be ascribed to the higher energy consumption to process the water at high pressures despite the higher mass of pollutant being degraded. The last consideration points out the chance of optimizing the system by varying the geometry and the recovery pressure.

In this paper, an attempt is made to find an explanation by a numerical simulation of the single- bubble dynamics (Eqs. (1–5)). In Fig. 4, the bubble radius and temperature (dimensionless value) are plotted against the distance downstream the orifice (for a water temperature $T = 293\,K$ and a bubble of initial radius $R_0 = 5\,\mu m$). The geometrical parameters—and consequently $A(x)$ (Eq. (4)), which influences the pressure profile $p_l(x)$ across the divergent section—chosen for the numerical simulation were the same as in the Venturi test for comparison sake. Fig. 4 reports the simulation at $p_1 = 0.65\,MPa$ and two different recovery pressures $p_2 = 0.10\,MPa$ (Fig. 4(a)) and $p_2 = 0.33\,MPa$ (Fig. 4(b)). It clearly shows that an increase in the recovery pressure enhances the violence of collapse (temperature peaks in Fig. 4(b)) and, therefore, the chemical reaction rate and the OH radical production. Macroscopically, it can be considered as the main reason explaining the positive effect of higher recovery pressure and recovery rate as underlined in the specialized literature [20]. A first -order reaction rate increasing with the temperature of the actual reaction zone is also suggested by the relevant work by Kotronarou et al. [18]. These authors put forward that, based on the nonvolatile and moderately hydrophilic behavior of pNP, the primary degradation mechanism is the thermal decomposition with the cleavage of the C–N bond in the boundary layer surrounding the collapsing bubble. Therefore, the behavior of the temperature peaks, shown in Fig. 4, can be rationally considered as the main reason for the effect observed at higher recovery rates of pressure.

5. Conclusions

The paper focuses on the effect of recovery pressure on pNP degradation by means of HC. At a fixed pressure drop, the increased recovery pressure results into more violent collapses and in the release of hydroxyl radicals, which explains the higher degradation rates of pNP, experimentally verified. The experiments proved that it can be convenient to investigate and optimize the recovery pressure and fluid dynamics downstream the constriction. A pNP mass removal of 40% was achieved at 30 min with an inlet pressure

of 0.70 MPa and a recovery one at 0.38 MPa (conversion per unit energy of 1.13 mg/MJ). These results underline the effectiveness of realizing cavitating geometries with a combination of conveniently designed in series constrictions. The mathematical model gave a theoretical insight on the empirical observations. Next investigations should also focus on the transport mechanisms and bubble population phenomena; further models will be developed directly to improve the configuration of multiple tandem Venturi (or equivalent cavitating geometries).

Nomenclature

A	—	area of the Venturi cross section [m^2]
C	—	pNP concentration [mg L^{-1}]
C_0	—	initial pNP concentration [mg L^{-1}]
C_v	—	cavitation number [dimensionless]
$C_{v,mix}$	—	heat capacity at constant volume of the gaseous-vapour mixture [J kg^{-1} K^{-1}]
C_w	—	concentration of water molecules in the bubble [mol m^{-3}]
C_{wR}	—	concentration of water molecules at the gas–liquid interface [mol m^{-3}]
D	—	diffusivity [cm^2 s^{-1}]
h	—	van der Waal's hard core radius [m]
h_w	—	enthalpy of water molecules [J mol^{-1}]
k	—	Boltzmann constant [m^2 kg s^{-2} K^{-1}]
L	—	length of the cavitating device [m]
l_{diff}	—	length scale of mass diffusion [m]
l_{th}	—	length scale of thermal diffusion [m]
n	—	number density of bubbles [#bubbles m^{-3}]
N_{tot}	—	total number of molecules (gas + vapor) in the bubble [mol]
N_w	—	number of water molecules [mol]
p_1	—	inlet pressure [Pa]
p_2	—	recovery pressure [Pa]
p_l	—	liquid total pressure [Pa]
p_v	—	water vapour pressure [Pa]
Q	—	volumetric flow rate [m^3s^{-1}]
R	—	bubble radius [m]
T	—	bubble temperature [K]
T_w	—	bulk liquid temperature [K]
U	—	instantaneous velocity [m s^{-1}]
u	—	mean velocity [m s^{-1}]
U_w	—	internal energy of water vapour molecules [J mol^{-1}]
V	—	solution volume [m^3]
x	—	independent variable—space [m]

Greek symbols

η	—	cavitation efficiency [mg MJ^{-1}]
λ	—	thermal conductivity of bubble contents [Wm^{-2}]
μ	—	viscosity [Pa s]
ρ	—	water density [kg m^{-3}]
σ	—	water surface tension [N m^{-1}]

References

[1] T.J. Mason, J.P. Lorimer, Applied Sonochemistry, Wiley-VCH Verlag GmbH, Weinheim, 2002.

[2] M. Capocelli, M. Prisciandaro, A. Lancia, D. Musmarra, Comparison between hydrodynamic and acoustic cavitation in microbial cell disruption, Chem. Eng. Trans. 38 (2014) 13–18.

[3] S. Li, L. Zhang, J. Wang, B. Wang, Y. Li, C. Ma, Degradation of congo red induced by air-bubbles in the presence of nanometer TiO_2 powders, Desalin. Water Treat. 51 (2013) 1–13.

[4] C.D. Wu, Z.L. Zhang, Y. Wu, L. Wang, L.J. Chen, Effects of operating parameters and additives on degradation of phenol in water by the combination of H2O2 and hydrodynamic cavitation, Desalin. Water Treat. 51 (2013) 1–7.

[5] M. Capocelli, E. Joyce, A. Lancia, T.J. Mason, D. Musmarra, M. Prisciandaro, Sonochemical degradation of estradiols: Incidence of ultrasonic frequency, Chem. Eng. J. 210 (2012) 9–17.

[6] M. Landi, V. Naddeo, V. Belgiorno, Influence of ultrasound on phenol removal by adsorption on granular activated carbon, Desalin. Water Treat. 23 (2010) 181–186.

[7] M. Capocelli, M. Prisciandaro, D. Musmarra, A. Lancia, Understanding the physics of advanced oxidation in a Venturi reactor, Chem. Eng. Trans. 32 (2013) 691–696.

[8] P.R. Gogate, G.S. Bhosale, Comparison of effectiveness of acoustic and hydrodynamic cavitation in combined treatment schemes for degradation of dye wastewaters, Chem. Eng. Process. 71 (2013) 59–69.

[9] M. Capocelli, M. Prisciandaro, A. Lancia, D. Musmarra, Hydrodynamic cavitation of p-nitrophenol: A theoretical and experimental insight, Chem. Eng. J. 254 (2014) 1–8.

[10] A.A. Pradhan, P.R. Gogate, Removal of p-Nitrophenol using hydrodynamic cavitation and Fenton chemistry at pilot scale operation, Chem. Eng. J. 156 (2010) 77–82.

[11] P.R. Gogate, S. Mededovic-Thagard, D. McGuire, G. Chapas, J. Blackmon, R. Cathey, Hybrid reactor based on combined cavitation and ozonation: From concept to practical reality, Ultrason. Sonochem. 21 (2014) 590–598.

[12] P. Kumar, S. Khanna, V. Moholkar, Flow regime maps and optimization thereby of hydrodynamic cavitation reactors, AIChE J. 58 (2012) 3858–3866.

[13] M. Capocelli, M. Prisciandaro, A. Lancia, D. Musmarra, Modeling of cavitation as an advanced wastewater treatment, Desalin. Water Treat. 51 (2013) 1609–1614.

[14] V.S. Moholkar, A.B. Pandit, Bubble behavior in hydrodynamic cavitation: Effect of turbulence, AIChE J. 43 (1997) 1641–1648.

[15] M. Capocelli, D. Musmarra, M. Prisciandaro, A. Lancia, Chemical effect of hydrodynamic cavitation: Simulation and experimental comparison, AIChE J. 60 (2014) 2566–2572.

[16] A. Sharma, P.G. Gogate, A. Mahulkar, A.B. Pandit, Modeling of hydrodynamic cavitation reactors based on orifice plates considering hydrodynamics and chemical reactions occurring in bubble, Chem. Eng. J. 143 (2008) 201–209.

[17] J.S. Krishnan, P. Dwivedi, V.S. Moholkar, Numerical investigation into the chemistry induced by hydrodynamic cavitation, Ind. Eng. Chem. Res. 45 (2006) 1493–1504.
[18] A. Kotronarou, G. Mills, M.R. Hoffmann, Ultrasonic irradiation of p-nitrophenol in aqueous solution, J. Phys. Chem. 95 (1991) 3630–3638.
[19] R.K. Joshi, P.R. Gogate, Degradation of dichlorvos using hydrodynamic cavitation based treatment strategies, Ultrason. Sonochem. 19 (2012) 532–539.
[20] P.R. Gogate, A.B. Pandit, Engineering design methods for cavitation reactors II: hydrodynamic cavitation, AIChE J. 46 (2000) 1641–1649.